

Subrecoil Raman spectroscopy of cold cesium atoms

J. Ringot, P. Szriftgiser, and J. C. Garreau

Laboratoire de Physique des Lasers, Atomes et Molécules and Centre d'Etudes et de Recherches Laser et Applications,
 Université des Sciences et Technologies de Lille, F-59655 Villeneuve d'Ascq Cedex, France

(Received 28 July 2001; published 11 December 2001)

We describe and characterize a setup for subrecoil stimulated Raman spectroscopy of cold cesium atoms. We study in particular the performances of a method designed for active control and stabilization of the magnetic fields across a cold-atom cloud inside a small vacuum cell. The performance of the setup is monitored by *copropagative-beam* stimulated Raman spectroscopy of a cold cesium sample. The root-mean-square value of the residual magnetic field is 300 μG , with a compensation bandwidth of 500 Hz. The shape of the observed spectra is theoretically interpreted and compares very well to numerically generated spectra.

DOI: 10.1103/PhysRevA.65.013403

PACS number(s): 42.50.Vk, 32.80.Pj, 32.60.+i

I. INTRODUCTION

Stimulated Raman spectroscopy has become in recent years one of the most useful and powerful tools for laser manipulation of cold atoms. Raman stimulated transitions have been used, for example, in subrecoil laser cooling [1]; for the preparation of Bloch states in a stationary wave [2]; to perform “sideband” cooling of trapped atoms [3]; and in subrecoil-precision measurement of atomic velocity distributions in quantum chaos experiments [4]. This powerful technique is however plagued by its sensitivity to stray magnetic fields that should imperatively be compensated for. In the present paper, we describe a setup used in the above mentioned quantum chaos experiment for subrecoil-precision measurements of velocity distributions of cold atoms, with a special emphasis in a method for reducing stray magnetic fields to a submilligauss level by active compensation.

All experiments reported below were done with cesium atoms, widely used in the present context, but most conclusions drawn in the present paper can be applied to other atomic species. Cesium recoil velocity v_r (i.e., the velocity acquired by an atom emitting or absorbing a single photon) corresponding to the usual D_2 line near 852 nm is 3.5 mm/s. The Doppler shift associated with a stimulated Raman transition at such a velocity is 8.4 kHz.

Let us briefly review some relevant features of the Raman stimulated spectroscopy. In the present context, Raman stimulated transitions (Fig. 1) are *two-photon* transitions connecting one hyperfine sublevel of the ground state to the other one by the absorption of a single photon in one Raman beam of frequency ω_1 and wave vector \mathbf{k}_1 and by *stimulated* emission of a photon in the other beam (frequency ω_2 and wave vector \mathbf{k}_2) *via* a virtual excited level. The Raman process is resonant if the frequency difference of the two Raman beams and the ground-state hyperfine interval ($\omega_{hf} \approx 2\pi \times 9.2$ GHz for cesium) are equal, and the Raman detuning for zero magnetic field, low-laser intensity, and zero-velocity atoms is defined as

$$\delta_R = \omega_1 - \omega_2 - \omega_{hf}. \quad (1)$$

We suppose that the Raman beams are either parallel or antiparallel. In what follows, we shall neglect $|k_1| - |k_2|$

$\approx |\omega_1 - \omega_2|/c$ compared to ω_1/c or ω_2/c , and take $k \equiv \omega_1/c \approx \omega_2/c$. If the Raman beams are counterpropagating (i.e., $k_1 \approx -k_2$), the detuning seen by an atom of velocity v is $\delta_R + 2k(v + v_r)$, the atomic velocity sensitivity of the transition is maximum and so is the momentum exchange between the Raman beams and the atom. This last property provides a way to perform subrecoil cooling [1]. On the other hand, if the two Raman beams have the same propagation direction (i.e., $k_1 \approx k_2$) the Raman detuning is almost insensitive to the atomic velocity. As sensitivity to magnetic fields and to light shifts is still present, copropagating Raman spectroscopy is very useful for the calibration of the apparatus.

Since the life time of the $F=4$ sublevel is very long (several thousands of years in the absence of collisions), the width of the Raman stimulated transitions will be, in principle, limited by Heisenberg's uncertainty principle. The transitions linewidths are thus proportional to the inverse of the excitation duration. For instance, a Raman pulse duration of about 20 μs , in the counter-propagating configuration, leads to a velocity resolution of v_r . If the amplitude of the pulse is adjusted to produce a π pulse, it will transfer a whole velocity class of width of v_r , centered at the velocity $v_0 = \delta_R/2k + v_r$ from one hyperfine sublevel to the other one. One may then reconstruct the atomic velocity distribution by measuring the transferred atomic population as a function of

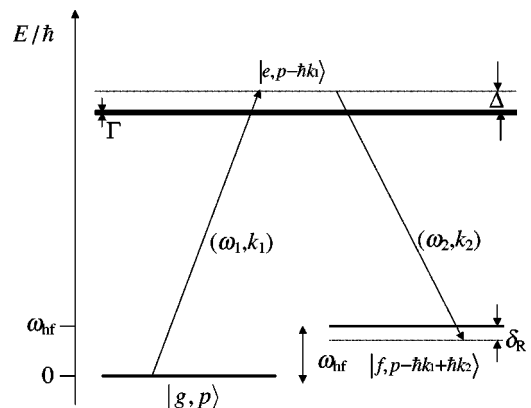


FIG. 1. Raman stimulated transitions. The two hyperfine ground-state sublevels are connected by a two-photon transition *via* a virtual intermediate level.

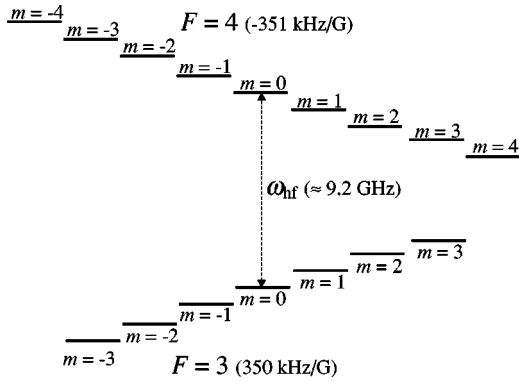


FIG. 2. Hyperfine structure of the cesium atom ground state in the presence of a magnetic field.

the Raman detuning δ_R . Finally, in order to prevent resonant transitions to (and spontaneous emission from) the excited state, the virtual intermediate level must lie far enough from the closest excited level, what can be achieved by choosing an optical detuning Δ much larger than the linewidth of the closest excited level. Typically $\Delta = 2\pi \times 200$ GHz in our experiment, to be compared to the $\Gamma = 2\pi \times 5.3$ MHz linewidth of the excited level. The spontaneous emission rate is thus reduced by about nine orders of magnitude with respect to the resonance. This is true in the limit of a narrow laser line; we have, however, noticed that power diode lasers present a large spectral background about 40 dB below the peak intensity that limits the reduction of the spontaneous emission rate.

The optical part of our Raman setup has been described in detail elsewhere [5]. Briefly, the Raman frequencies are generated by direct current modulation at 4.6 GHz of a diode laser. The current modulation generates two optical sidebands separated by 9.2 GHz that are used to perform injection lock of two independent power diode lasers. We obtain in this way two 150 mW laser beams with the required frequency separation and with a beat-note width below 1 Hz. The Raman beams then pass through three acousto-optical modulators acting as optical switches that control the interaction time and allow shifting from the co- to the counter-propagating beam configuration. Finally, the resulting beams are transported by monomode, polarization maintaining, optical fibers to the region of interaction with the atomic cloud.

II. ACTIVE COMPENSATION OF THE MAGNETIC FIELD

The ground state of cesium splits into two hyperfine sublevels $F=3$ and 4 separated by 9.2 GHz (the cesium-clock frequency). The linear Zeeman split for these states is of the form $Z_F B m_F$, where B is the magnetic field, m_F the azimuthal quantum number, and Z_F the Zeeman coefficient (around 350 kHz/G in modulus) (Fig. 2). An atom in the $F=4$ hyperfine sublevel undergoing a 6 mG magnetic field (2% of the Earth's mean magnetic field) will experience a Zeeman shift equal to the recoil velocity Doppler shift. Thus, in order to perform atomic velocity manipulation with sub-recoil resolution, the magnetic field should be reduced at least to the mG level. Usually, this is done by shielding the

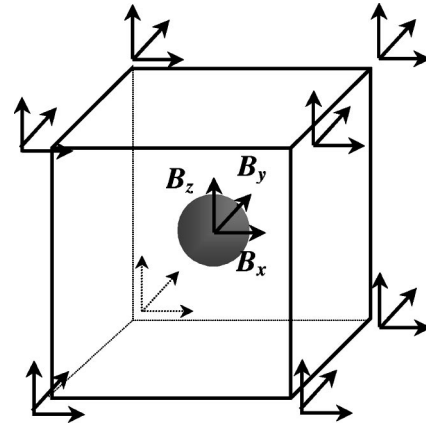


FIG. 3. Schematic representation of the probe geometry around the vacuum cell. The compensating coils are not shown.

experimental zone with a double “mu-metal” sheet providing a high degree of isolation against magnetic fields. However, the shield reduces the optical access to the experiment and, as mu-metal is difficult to tool, it also tends to forbid further evolution of the setup. Furthermore, the magnetic gradient of a magneto-optical trap magnetizes the shield on the scale of a day, leading to a slow magnetic field drift. It is thus interesting to perform an acceptable field reduction without any “physical” shield. In general the local magnetic field across the experiment is a sum of several components: dc earth field; dc stray fields, e.g., from an ion-pump permanent magnet; ac components from the line (50 or 60 Hz) and its harmonics; etc. This means that the magnetic-field configuration is greatly dependent on the particular setup one wants to protect, and that a dc magnetic field compensation alone is insufficient.

To overcome most of those problems, the method we describe here is to perform a real-time compensation of the magnetic field in the three directions with, for each direction, dc and ac compensations. In order to do so, we use the fact that the sum of the magnetic fields at the eight corners of a cube gives eight times the magnetic field at the center of this cube. This result is independent of the gradient of the field, and the first nonvanishing correction is of second order in the magnetic field. One should, nevertheless, noticed that this statement is valid only for the exact geometric center of the cube. If the magnetic gradient is too high, the spatial extension of the atomic cloud may lead to an important broadening due to the inhomogeneity of the residual magnetic field. We will come back to this point at the end of the section.

In practice, we placed 24 magneto-resistive probes at the eight corners of the vacuum cell, three at each corner oriented according to the three orthogonal directions (see Fig. 3). The probes are mounted on two U-shaped integrated circuits placed parallel to the top and bottom faces of the cell, preserving a large optical access to the cell. A maximum of algebraic operations is performed directly by the integrated circuits in order to reduce the number of external electric connections. The sum of the eight signals for a given direction generates the error signal corresponding to that direction. We generate in this way three error signals that are integrated and used to drive current supplies (we simply use

standard diode laser supplies in our setup) *via* a modulation input. Each supply in turn drives a coil pair in Helmholtz configuration generating a magnetic field opposite to that measured by the probes. The rectangular compensating coils are typically 1.5 meter wide in order to insure the homogeneity of the compensated magnetic field across the vacuum cell (whose size is 10 cm). The magneto-resistive probes (HMC2003 Honeywell) have, according to the manufacturer data, a resolution better than $40 \mu\text{G}$. In closed-loop operation, the residual magnetic-field fluctuation measured by the probes is $150 \mu\text{G}$, corresponding to a reduction of one order of magnitude of the ac component, and the bandwidth is better than 500 Hz. We took care of aligning the probes axes with the axes of the compensation coils to better than five degrees, and we never saw any instabilities due to the coupling among the three directions when the three servo-loops act simultaneously. With this setup, we verified that if one scans the dc magnetic-field component along one direction (by scanning the respective dc current) the stability of the compensation along the other directions is not affected.

A good way of testing the effectiveness of our setup is to perform *copropagating* Raman spectroscopy. We have seen in Sec. I that such a configuration is almost insensitive to the atomic velocity, and it allows easy diagnostic of perturbing effects such as residual magnetic fields and light shifts. To do so, we programmed our experiment to execute the following time sequence: The magneto-optical (MOT) trap is loaded; the MOT gradient of magnetic field is shut down and a ‘‘Sisyphus’’ sequence is applied for further cooling. Twenty milliseconds after cutting the MOT gradient, the magneto-resistive probes are reset. Resetting must be done before the probes can perform measurements once they have been submitted to intense magnetic fields (e.g., the MOT gradient). A special function is provided in the probe chip for this end. A few milliseconds later, the servo loops are switched on. After twenty milliseconds, the optical beams are shut down, the atoms are transferred from the $F=4$ to the $F=3$ sublevel, and the Raman pulse is applied. The Sisyphus sequence lasts for around 60 ms, which is longer than in other cold atom experiments (typically 30 ms), but is much shorter than the requested delay (around 200 ms) when a mu-metal shield is used, necessary to allow for the shield magnetization relaxation.

By applying a dc magnetic field during the experiment, one may perform spectroscopy of cesium ground-level Zeeman states. If the dc field has no particular orientation with respect to the polarizations of the Raman beams [6], the selection rules for the Raman transitions are $\Delta m=0, \pm 1, \pm 2$. As the Zeeman coefficients for $F=3$ and 4 are almost equal and have opposite signs, $Z_3=350 \text{ kHz/G}$ and $Z_4=-351 \text{ kHz/G}$, the position (with respect to the line center) of the line connecting the sublevels $(3,m)$ and $(4,m')$ is

$$\Delta \nu(m,m') \text{ (kHz)} = [350(m+m') + m']B \text{ (G)}. \quad (2)$$

As we are dealing with weak magnetic fields, the second term in the brackets is in general negligible, and we may consider that the position of the lines depends only on $m+m'$. One easily deduces that the spectrum can display up to

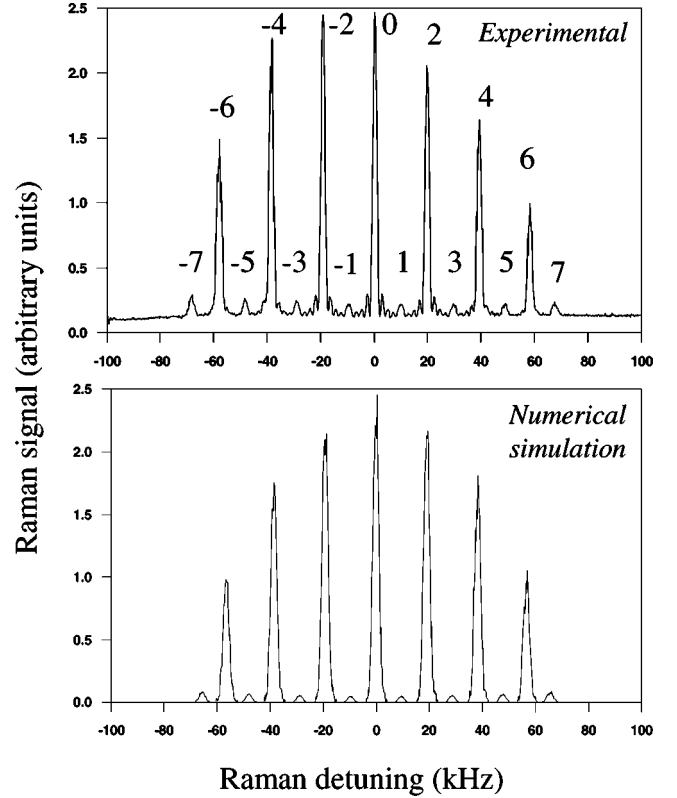


FIG. 4. Experimental and numerically generated (see Sec. III) Zeeman spectra of Raman transitions in cesium. The lines of small intensity correspond to transitions $\Delta m = \pm 1$, showing that the dc field is almost parallel to the Raman beams wave vector \mathbf{k} . The numerical simulation was made with $B_0=28 \text{ mG}$, $\Delta B_0=0.5 \text{ mG}$, $\Delta I_0/I_0=0.025$, and $\theta_0=0.2 \text{ rad}$. The asymmetry of the experimental spectrum is due to the fact that the Zeeman sublevels of the initial level are not equally populated.

15 lines, as shown in Fig. 4. This figure has been obtained by applying a dc field of 28 mG with the magnetic-field compensation setup described above active. The Raman pulse duration is $500 \mu\text{s}$. In Fig. 5, we compare a ‘‘zoom’’ of the line noted -6 in Fig. 4 with the magnetic-field active compensation on and off, clearly showing a noise reduction effect. When the ac compensation is shut off, the dc component remains.

The maximum measured full width at half maximum (FWHM) of the lines in Fig. 4 is 1.5 kHz. For longer interaction times, we have observed a linewidth of 600 Hz that corresponds to a velocity resolution better than $v_r/10$ and thus to a field residual amplitude of $300 \mu\text{G}$. Achieving this last value was only possible by taking into account the fact that the atomic cloud has a spatial extension and sees a residual magnetic gradient. We thus added a static gradient-compensating coil pair in an anti-Helmholtz configuration with the same axis as the MOT gradient coils. The current of those coil was adjusted in order to reduce the linewidth. The minimum width has been achieved for a nonzero compensating gradient value, around 10 mG/cm . This also sets a maximum value for the residual magnetic gradient of 10 mG/cm .

Reducing the dc field leads to a collapsed, Zeeman-compensated spectrum, with a FWHM of about 4 kHz (see

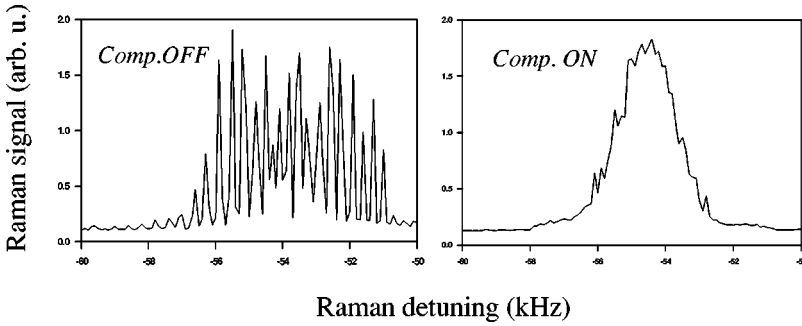


FIG. 5. Detail of the line -6 of Fig. 4 with the active compensation off and on. The noncompensated curve presents a noise level close to 100%. The regular oscillations superimposed on the line itself are due to a stroboscopic effect between the network frequency (50 Hz) and the repetition rate of the measurements (4 Hz).

Fig. 6). In principle, one would expect the width of the collapsed spectrum to be just slightly greater than the widest line of the split spectrum. Explaining this “unexpected” broadening is the purpose of the next section.

With the performances described above, we easily achieved a velocity-measurement resolution of $v_r/2$. As an example, Fig. 7 presents a measurement of the velocity distribution of the cesium atoms. The FWHM is 82 kHz, corresponding to a temperature of $3.3 \mu\text{K}$ which is typical of “Sisyphus-boosted” MOTs. This proves the ability of the setup to perform subrecoil spectroscopy.

Concluding this section, we can say that this setup displays a sufficient resolution to be used in most Raman stimulated spectroscopy experiments. Furthermore, there is hardly any reduction of the optical access to the vacuum cell. Let us mention that the setup presents an annoying limitation in the

everyday use. We observed that the HMC2003 probes present a slow drift, with a time constant of roughly one hour. This implies that the dc compensation current has to be corrected to compensate the drift of the probes. We accounted for this effect by a software procedure that sweeps the dc current in order to restore a fixed value of the magnetic field (as measured by the probes), for instance each hour. In fact we verified that the dc magnetic field itself is very stable on the time scale of a day. This opens the possibility of replacing the magneto-resistive probes by small coils and use the induction signal to generate an ac error signal, and to compensate only the ac fluctuations. The stable dc component is corrected by a constant dc current that is adjusted at the beginning of the experiment. Preliminary tests indicate that this technique presents no measurable drift.

III. STUDY OF THE SPECTRA

The relative intensity of the Raman transitions depends on the Raman amplitude connecting the respective Zeeman sublevels, which is proportional to the product of the dipole matrix elements connecting each sublevel to the concerned intermediate excited level (see the Appendix). The position of each Zeeman sublevel depends on the magnetic field and on the intensity of the Raman beams through the light shift, which, for the far detuned Raman beams we are considering here, depends only on the dipole matrix element connecting

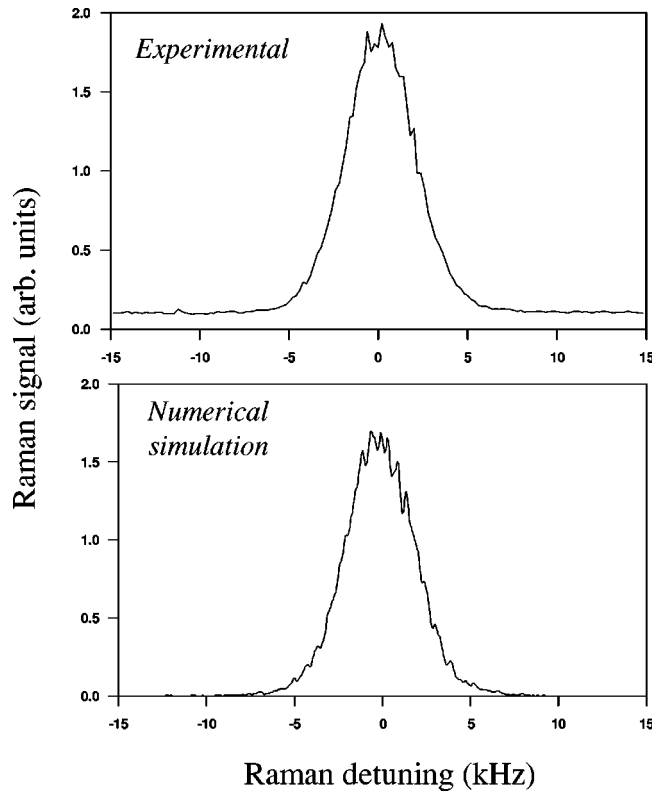


FIG. 6. Collapsed Raman spectrum at low magnetic field (FWHM 4.5 kHz). Comparison with the corresponding spectrum obtained by numerical simulation (see Sec. III), obtained with $B_0 = 0.5 \text{ mG}$, $\Delta B_0 = 0.3 \text{ mG}$, $\Delta I_0/I_0 = 0.027$, and $\theta_0 = 0.1 \text{ rad}$.

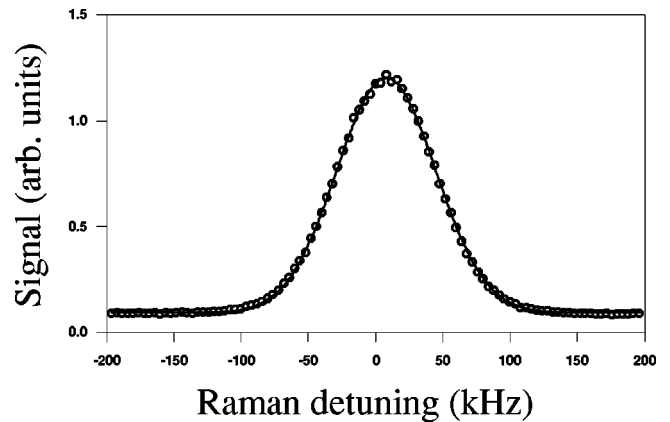


FIG. 7. Velocity distribution of cooled cesium atoms. The FWHM is 82 kHz, corresponding to a temperature of $3.3 \mu\text{K}$, deduced from the Gaussian fit. The resolution is of $v_r/2$ (or, equivalently, 4.2 kHz), showing the ability of the setup to perform subrecoil spectroscopy.

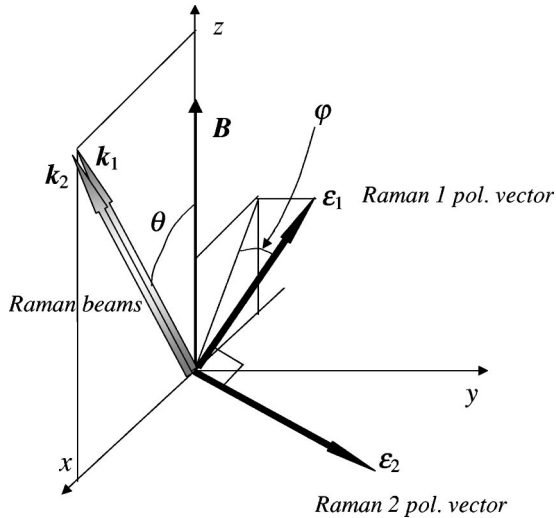


FIG. 8. Geometry of the Raman beams and the magnetic field.

the considered Zeeman sublevel to the excited level. We choose the magnetic-field \mathbf{B} to be parallel to the quantization axis, labeled \mathbf{z} . The Raman beams are copropagating with wave-vector \mathbf{k} (see Fig. 8), and lie in the $(x-z)$ plane, making an angle θ with respect to the \mathbf{z} axis. The (orthogonal) polarization vectors associated with the two Raman beams lie in a plane orthogonal to \mathbf{k} , and the polarization of the Raman beam starting from the level $F=3$ makes an angle φ with the $(x-z)$ plane (this last angle is irrelevant for our problem and we always take $\varphi=0$ in what follows).

We consider three main causes of line broadening: (a) magnetic-field fluctuations and inhomogeneities, (b) fluctuations and inhomogeneities of the intensity of the Raman beams, and (c), the finite duration of the pulses. We shall consider each of these effects in detail.

The fluctuations of the magnetic field displace the Zeeman sublevels, and thus, displace the center of each Raman line (except the line connecting the Zeeman $m=m'=0$ sublevels, if allowed). Furthermore, we consider that the magnetic field in our setup results from the vectorial addition of a controlled, dc vector \mathbf{B}_0 and of a randomly fluctuating component $\Delta\mathbf{B}$. The resulting magnetic field thus varies both in modulus and in direction. The quantization axis is aligned with the dc component. The spatial inhomogeneity of the magnetic field also displaces the position of the Raman lines, thus contributing to the inhomogeneous broadening. We do not know the exact shape of the magnetic field over the atomic cloud, but as the atoms have an almost random spatial distribution, this contribution can be statistically treated in the same way as a field fluctuation and we do not distinguish between them. The typical magnitude of this effect in the weak-magnetic-field regime is 1.5 kHz.

The dominant low-magnetic-field broadening factor is the fluctuation of the light shifts (as for the magnetic-field effect, we do not distinguish the contributions of fluctuations and of inhomogeneities). These fluctuations are in part due to the fluctuations of the intensity of the Raman beams themselves. However, the light shift affecting a given Zeeman sublevel (F, m) is independent of F and m if the direction of the

magnetic field is parallel to the direction of propagation of the Raman beams ($\theta=0$). This result is also valid for zero magnetic field, as one may then always choose the quantization axis parallel to the beams. This implies that the light-shift fluctuations in this configuration displace the lines as a whole, and cannot contribute to the broadening of an individual line. This fact shall play an essential role in what follows. Thus, we do not expect the best compression of the spectrum to be achieved with zero dc field, because in this case, the fluctuating component $\Delta\mathbf{B}$ induces magnetic field random rotations with respect to \mathbf{k} , leading to spectra that are broad and asymmetric. The thinnest lines are expected to be obtained with a dc field parallel to the Raman beams of an amplitude a few times greater than the mean amplitude of the fluctuating component: in such a case, the fluctuation of the magnetic field induces only small misalignments with respect to propagation direction of the Raman beams. We verified these facts both experimentally and numerically (see below). Let us mention that a simple way to obtain the alignment of the dc field and the Raman beams is to try to minimize the amplitude of the lines corresponding to $\Delta m = \pm 1$ (that is, $-7, -5, \dots, 5, 7$) in the spectrum of Fig. 4, as the Raman selection rules forbid such transitions if \mathbf{B} and \mathbf{k} are parallel. If the axes of the compensation coils are aligned with the Raman beams (as it is the case in our setup), one may reduce the dc component without losing the correct field orientation.

We verified that lowering the intensity of the Raman beams produces thinner linewidths, confirming the dominant role of the light-shift broadening. The intensity used in our quantum chaos experiment [4] and in the curves shown in the present paper is 20 mW for each Raman beam of waist 4 mm. The typical value of the broadening associated with the light-shift fluctuations is 3.5 kHz.

The last broadening effect is the finite duration of the Raman pulses. We worked with Raman pulses ranging from 1 to 3 ms for which the associated broadening (around 0.2 kHz) is negligible.

Numerically calculated spectra have been generated by a Monte Carlo technique. A particular value for the magnetic field is generated by adding a fixed dc component \mathbf{B}_0 making an angle θ_0 with \mathbf{k} and a perturbation $\Delta\mathbf{B}$, whose amplitude is picked from a Gaussian distribution of zero mean, root-mean-square amplitude ΔB_0 , and of random orientation. Note that ΔB_0 is formed by two contributions: the stray local fields (independent of B_0) and the fluctuations of B_0 itself, which we assume to be proportional to B_0 (due, e.g., to fluctuations of the current delivered by the supplies).

In the same way, a value for the intensity of each Raman beam is picked from a Gaussian distribution of mean intensity I_0 and root-mean-square variation ΔI_0 . The position and the amplitude of each line is then calculated, and a particular spectrum generated using the Fourier-transform-limited linewidth given by the inverse of the pulse duration. Typically, 1000 of such randomized spectra are averaged to produce the numerical spectra shown in Figs. 4 and 6.

As expected, the best collapsed spectrum is obtained for a nonzero value of the dc field. Figure 9 displays the numerically calculated dependence of the FWHM on the dc mag-

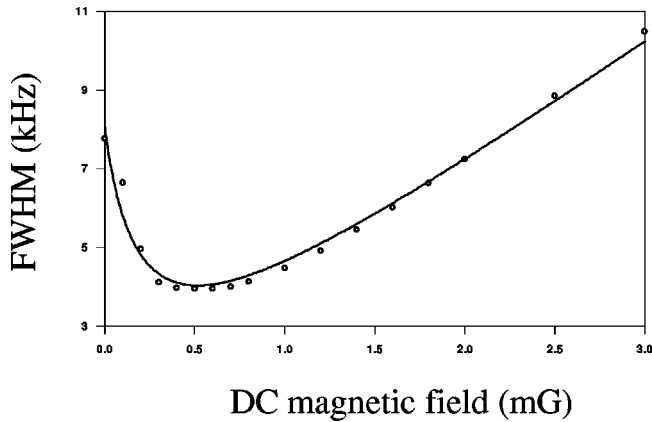


FIG. 9. Theoretical FWHM of the collapsed spectrum as a function of the applied dc field. The fitting curve is $1.74/(B_0+0.21) + 3.24B_0$, with B_0 in mG.

netic field B_0 , showing a well-defined minimum around $B_0 = 0.5$ mG. For stronger mean fields, the broadening is dominated by the fluctuations of B_0 itself, and should be linear in B_0 . For values of B_0 close to zero, the broadening is due essentially to field rotations induced by the fluctuation component. The fluctuations of the field direction are roughly proportional to $\Delta B_0/B_0$ and the related broadening is maximum if $B_0=0$, but it cannot be infinite. We thus write the weak field term as $A/(B_0+b)$, where A/b is the zero dc field broadening, depending only on ΔB_0 . Thus, the shape of the curve shall be

$$F(B_0) = \frac{A}{B_0+b} + CB_0. \quad (3)$$

Figure 9 shows that this form fits rather well the numerical simulation. Unfortunately, we cannot directly compare this result to experimental data as we do not have an independent measurement of the mean magnetic field across the atomic cloud.

Interestingly, one also finds that the minimum width does not correspond to $\theta=0$ (perfect alignment of the magnetic field and the Raman beam wave vector) but to a small angle $\theta_0=0.1$ rad. For such an angle, light shifts are slightly different for each Zeeman sublevel, and so are the Zeeman shifts. We attribute the minimum to a partial compensation of the two effects. This misaligned configuration tends to produce asymmetric spectra, which has also been observed experimentally.

Concluding this section, we may say that we have provided an interpretation of the physical mechanisms governing the width of the Raman lines. The interpretation has been tested by comparing numerically generated spectra to the experimental results, which allowed us to quantify the performances of our setup. Moreover, the interpretation furnishes some interesting hints for the minimization of the width of the collapsed spectra. The fact that the FWHM of the collapsed spectrum decreases as one decreases the Raman beam intensities (which indicates the dominant role of the light-shift fluctuations), and the fact that the best collapse is ob-

tained with a nonzero magnetic field aligned with the direction of the Raman beams (which indicates that magnetic-field misalignment with respect to the beams plays an essential role), constitute further support of our interpretation of the shape of the spectra. Both these facts have been verified experimentally. Another interesting idea is to polarize the atoms in one of the extreme ($|m|=F$) Zeeman sublevels by optical pumping. This shall sensibly reduce the broadening due to fluctuations of the light shift. Based on the measurements we have done in the split spectrum configuration, we expect in this case a collapsed linewidth of the order of 1 kHz.

IV. CONCLUSION

We presented in this paper an experimental setup for sub-recoil stimulated Raman spectroscopy. A key feature of the setup is the active compensation of magnetic fields over a small volume. Sensitive Raman stimulated transitions on cesium have been used to characterize the setup, with residual magnetic field fluctuations of 0.3 mG. The final limit of the method has been shown to be related to lightshift fluctuations rather than to the magnetic field ones. The residual linewidth is 4 kHz, provided a small nonzero dc field is kept, allowing atomic velocity selection of $v_R/2$. Carefully constructed Raman π pulses would allow us to reduce the light power, pushing the resolution on the atomic velocity selection to the $v_R/10$ level, which would be comparable to the results obtained with double mu-metal shielding [2].

ACKNOWLEDGMENTS

Laboratoire de Physique des Lasers, Atomes et Molécules (PhLAM) is UMR 8523 du CNRS et de l'Université des Sciences et Technologies de Lille. Center d'Etudes et Recherches Lasers et Applications (CERLA) is supported by Ministère de la Recherche, Région Nord-Pas de Calais, and Fonds Européen de Développement Economique des Régions (FEDER).

APPENDIX: LIGHT SHIFTS AND TRANSITION RATE COEFFICIENTS

The geometry and definitions used in this appendix are those of Fig. 8, explained in Sec. III. We choose the quantization axis parallel to the magnetic field and decompose the polarizations of the Raman beams in irreducible components (noted ϵ_- , ϵ_0 , ϵ_+) with respect to that axis [6]

$$\begin{aligned} \epsilon_{1-} &= \frac{-\cos \varphi \cos \theta + i \sin \varphi}{\sqrt{2}}, \\ \epsilon_{10} &= \cos \varphi \sin \theta, \quad \epsilon_{1+} = \frac{\cos \varphi \cos \theta + i \sin \varphi}{\sqrt{2}}, \end{aligned} \quad (A1)$$

and the components of the polarization vector ϵ_2 of the second beam are obtained by changing φ into $\pi/2 - \varphi$.

The light shift of the sublevel (F, m) induced by the beam labeled i ($i=1,2$) is proportional to

$L_i(F, M)$

$$= (qE_i)^2 \sum_{F'} \frac{\left| \sum_p \langle 6S_{1/2} F m | r_p \epsilon_{ip} | 6P_{3/2} F' m - p \rangle \right|^2}{\Delta_i(F, M; F', M')}, \quad (\text{A2})$$

where q is the electron charge, E_i the electric field associated to the i Raman beam, $p = \{-, 0, +\}$, r_p is the irreducible p

component of the position vector, and (F', m') correspond to the Zeeman sublevels of the excited state ($F' = 2, 3, 4$ if $F = 3$ and $F' = 3, 4, 5$ if $F = 4$), and $\Delta_i(F, m, F', m')$ is the optical detuning. For simplicity, we will consider that the optical detuning is high enough so that the above value may be considered to be independent of the sublevel (practically, this means that the optical detuning must be much larger than 250 MHz). Applying the Wigner-Eckart theorem, one may reduce the above equation to the more useful form:

$$L_i(F, m) = (qE_i)^2 \sqrt{2} (2F+1)(2J+1) \frac{|\langle 6S_{1/2} || \mathbf{r} || 6P_J \rangle|^2}{\Delta} \sum_{F'} \left| \sum_p \epsilon_{ip} \sqrt{2F'+1} \begin{Bmatrix} 1/2 & J & 1 \\ F' & F & 7/2 \end{Bmatrix} \begin{pmatrix} F' & 1 & F \\ m-p & p & -m \end{pmatrix} \right|^2, \quad (\text{A3})$$

where the symbol in brackets is the reduced matrix element of \mathbf{r} , the symbol in braces a “6j” symbol, and the symbol in parentheses is a “3j” symbol [7]. The total light shift $L(F, m)$ affecting the sublevel (F, m) is thus obtained by adding the contributions due to each Raman beam.

Let us now consider the Raman transition amplitude $(F_1, m_1) \rightarrow (F_2, m_2)$, which is proportional to

$$\sum_{F'} \sum_p \sum_{p'} \langle 6S_{1/2} F_1 m_1 | r_p \epsilon_{1p} | 6P_{3/2} F' m_1 - p \rangle \langle 6P_{3/2} F' m_1 - p | r_{p'} \epsilon_{2p'} | 6S_{1/2} F_2 m_1 - p - p' \rangle \quad (\text{A4})$$

that can be transformed into

$$\begin{aligned} & |\langle 6S_{1/2} || \mathbf{r} || 6P_J \rangle|^2 (-1)^{F_1+F_2-q-J+1/2} \sqrt{2} (2F_1+1)(2F_2+1)(2J+1) \sum_p \sum_{p'} \epsilon_{1p} \epsilon_{2p'} \begin{Bmatrix} 0 & 1 & 1 \\ J & 1/2 & 1/2 \end{Bmatrix}^2 \sum_{F'} (2F'+1) \\ & \times \begin{Bmatrix} 1/2 & J & 1 \\ F' & F_1 & 7/2 \end{Bmatrix} \begin{Bmatrix} J & 1/2 & 1 \\ F_2 & F' & 7/2 \end{Bmatrix} \begin{pmatrix} F' & 1 & F_1 \\ m_1-p & p & -m_1 \end{pmatrix} \begin{pmatrix} F_2 & 1 & F' \\ m_1-p-p' & p' & -(m_1-p) \end{pmatrix}. \quad (\text{A5}) \end{aligned}$$

- [1] M. Kasevich and S. Chu, Phys. Rev. Lett. **69**, 1741 (1992).
 [2] M. Ben Dahan, E. Peik, J. Reichel, Y. Castin, and C. Salomon, Phys. Rev. Lett. **76**, 4508 (1996).
 [3] V. Vuletic, C. Chin, A. J. Kerman, and S. Chu, Phys. Rev. Lett. **81**, 5768 (1998); M. Morinaga, I. Bouchoule, J. C. Karam, and C. Salomon, *ibid.* **83**, 4037 (1999).
 [4] J. Ringot, P. Szriftgiser, J. C. Garreau, and D. Delande, Phys. Rev. Lett. **85**, 2741 (2000).
 [5] J. Ringot, Y. Lecoq, J. C. Garreau, and P. Szriftgiser, Eur. Phys. J. D **7**, 285 (1999).
 [6] We work with Raman beams of orthogonal polarizations; as, for beams far detuned from the optical resonance, the transi-

tion probability with parallel polarizations is zero. This is due to symmetry properties of the Clebsch-Gordan coefficients when summed over all hyperfine sublevels of the intermediate level $6P_{3/2}$.

- [7] Definitions and very useful formulas for calculation of these symbols may be found in Chap. 14 of I.D. Landau and E.M. Lifshitz, *Mécanique Quantique, Théorie Non Relativiste* (Mir, Moscow, 1966). Note that formulas (106,14), (108,10), and (106,10) of this reference are very well adapted for the numerical computation of “3j,” “6j” symbols and Clebsch-Gordon coefficients.